Title
RoboLase: A Robotic Laser Scissors and Lasertweezers Microscope

ISBN
978-1-4244-0784-2

Authors
Shi, Linda Z
Nascimento, Jaclyn M
Wakida, Nicole
et al.

Publication Date
2006-10-01

DOI
10.1109/acssc.2006.356609

"RoboLase": A robotic laser scissors and laser tweezers microscope

Linda Z. Shi*, Jaclyn M. Nascimento, Nicole Wakida, Alexander Dvornikov, Norman Baker, Elliot L. Botvinick and Michael W. Berns

***Abstract*—We have built a robotic laser scissors and laser tweezers microscope ("RoboLase") that can be operated via the internet. The system can be used to image, ablate, and/or trap cells and their organelles by remote-control. In the ablation mode, RoboLase is being used to perform delicate microsurgery on mitotic organelles (individual microtubules, spindle fibers, and centrioles). In the trapping mode, the system is being used as a real-time automatic tracking and trapping system (RATTS) of fast moving cells. RATTS performs all tracking and trapping functions without human intervention and has been used remotely between Australia and the US.**

***Index Terms*—laser scissors, laser tweezers, robotic microscope**

I. Introduction

Technology is revolutionizing the biomedical field with the latest development of automatic image processing algorithms and real-time robotic devices. Automated image processing algorithms have been successfully applied to tracking neurons (1-2), *Caenorhabditis elegans* (3), and sperm cells (4-5), identifying *Sphacelaria* algae (6) and soil bacteria (7), and reconstructing live embryos (8). Robotic telemicroscopy has been developed for general applications in (9-10) and is currently being applied to the pathology (11-13) and microsurgery (14-15).

Lasers are useful tools for micromanipulation of biological specimens (16). With the addition of tightly focused laser beams, microscopes have been turned into elaborate preparative tools that not only allow detailed observation of a specimen but also the capture, displacement, and microdissection of biological samples in vitro with astonishing ease and accuracy (17). Some commercial optical trapping and scissors systems are available, such as The LaserTweezers® Workstation and The LaserScissors® Workstation from Cell Robotics Inc, and PALM MicroLaser Systems from P.A.L.M. Microlaser Technologies.

Consistent with the need to develop sophisticated new nanosystem technologies, we have built a robotic laser scissors and laser tweezers microscope ("RoboLase") that can be remotely operated using either internet or dedicated line technology. The system can be used to image, ablate, and/or trap moving cells and their organelles. For the laser ablation application (Figure 1), the microscope stage, microscope parameters (reflector turret, light path, light intensity, objective selection and focus control), laser and arc lamp shutters, laser power, laser fire position, camera parameters and camera control are all controlled by the software. The user can draw multiple different shapes (dot, line, rectangle, circle, irregular shapes) on the captured cell image using the computer mouse. A click of a button on the computer screen instructs the laser to outline or cut out the shapes at the pre-set laser power. For the sequence acquiring image mode, the stage can be moved either by a joystick or by the computer mouse, and the objective focus can be adjusted by a mouse-click. For the time series mode, the phase or fluorescence images can be captured in a fixed-time interval and saved to the hard disk. The time series can also be paused if the interested cell is swimming out of focus. The histogram of the image is displayed on the computer screen to aid the user in adjusting the image display intensity by varying the maximum and minimum intensity values. For the laser trapping application, phase contrast images of swimming cells are digitized to the computer at a video rate (30 fps). The custom algorithm creates a region of interest (ROI) centered about a cell in response to a mouse click and performs all subsequent tasks automatically. Microscope stage movement responds to feedback from video analysis of the swimming cell to center the cell with respect to the field of view. The cell is automatically relocated to the laser trap focus where it is trapped either at a fixed power for a user-defined duration, or at a gradually decreasing laser power until the cell escapes. The cell's position is automatically monitored in order to measure the laser power at which the cell escapes the trap.

Manuscript received October 29, 2006. This work was supported in part by the Air force Office of Scientific Research (AFOSR # F9620-00-1-0371) to MWB, and the Beckman Laser Institute Foundation.

M. W. Berns is with Beckman Laser Institute and Department of Biomedical Engineering, University of California, Irvine, (phone: 949-824-7565; fax: (714) 824-8413; e-mail: mwberns@uci.edu).

L. Z. Shi, J. M. Nascimento, N. Baker, are with University of California, San Diego. Nicole Wakida, Alexander Dvornikov, Elliot Botvinick are with the Beckman Laser Institute University of California, Irvine.

II. Robotic Laser Ablation Microscope System

A. System setup

The detailed hardware setup of the robotic laser ablation microscope was described in (10), (18) and (19). Nearly

identical hardware and software setups (Figure 1) are placed in both biophotonics labs (one at University of California San Diego (UCSD)), Bioengineering Department/Whitaker Institute and one at University of California Irvine(UCI), Beckman Laser Institute). A laser (Coherent Mira 900 Ti:Sapphire laser (Coherent Inc, Santa Clara, CA) emitting 200 fs pulses at 76 MHz for ablation at 800 nm at UCI lab or a diode-pumped Spectra-Physics Vanguard laser with a second harmonic generator (SHG) providing a TEM00 mode 532 nm laser with a 76 MHz repetition rate, 30 ps pulse duration, and 2 W average power at UCSD) is focused into an inverted microscope (Zeiss Axiovert 200M) equipped with either a 40x oil numeral aperture (NA) 1.3 or a 63x oil NA 1.4 plan-apochromat PH3 oil objective. A Hamamatsu Orca-AG deep-cooled 1,344 × 1,024 pixel 12-bit digital CCD camera with digital (fire wire) output is mounted on the microscope to capture phase contrast and fluorescent images. A 7344 motion controller (PCI 7344, National Instruments, Houston, TX) is housed in a PCI slot of the host computer. A 4-axis stepper-motor driver (MID-7604, National Instruments) connected to the motion controller drives the x-y stepper-motor stage (LUDL Electronic Products LTD, Hawthorne, NY) of the microscope. A mechanical shutter (Uniblitz LS6ZM2, Vincent Associates, Rochester, NY) in the laser path and the front of arc lamp are controlled by a three-channel shutter driver (Uniblitz VMM-D3, Vincent Associates) through two lines of digital input-output from the motion controller respectively. A rotary stepper motor mount (PR50PP, Newport Corporation, Irvine, CA) housing a Glan laser linear polarizer is controlled by the motion controller and stepper motor driver to modulate the ablation power.

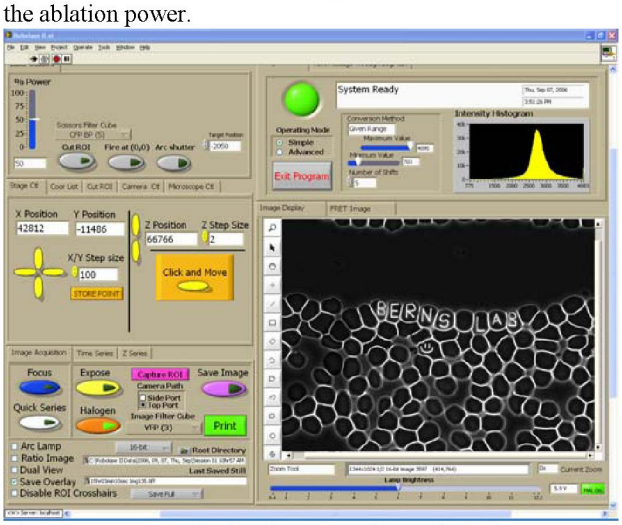

Figure 1 Front panel of RoboLase software in both UCSD and UCI labs

B. *Biological experiments*

The robotic laser ablation microscope system is used to perform nanosurgery of a single or whole spindle of microtubules in living cells as shown in (10), (17) and (18). A single microtubule from a live rat kangaroo kidney epithelial cell can be cleanly ablated with the femtosecond laser and the post-irradiation rate of depolymerization can be determined following the laser exposure (Figure 2). The fluorescent image of microtubules at the periphery of the cell is shown in Figure 2(a) (image cropped for publication). The single microtubule was moved to the center of the field of view and the crosshair was overlapped on top of the single microtubule as shown in Figure 2(b). The laser was fired at the crosshair position by pressing the "Fire at (0,0)" button from RoboLase software (Figure 1). The subsequent fluorescent images are the microtubule depolymerizing after 1 s (Figure 2(c)), 5 s (Figure 2(d)), 10 s (Figure 2(e)), and 15 s (Figure 2(f)).

The experiments using the robotic laser ablation microscope system have also shown that the immediate complete ablation across both half spindles (severing microtubule connections between pole and chromosome at the metaphase plate) after anaphase onset results in either the prevention or delay of cytokinesis. However, the chromosomes still undergo anaphase movements from the metaphase plate to the poles (Figure 3). Once the anaphase onset was observed using phase contrast in Figure 3(a) and the fluorescent image in Figure 3(b), the immediate two-line laser ablations on both ends near the poles were performed as shown in Figure 3 (c-d). The fluorescent image 90 seconds after laser ablation showed a recovery in Figure 3(e). The chromosomes still underwent anaphase movements from the metaphase plate to the poles as shown in the phase contrast image in Figure 3(f) and the fluorescent image in Figure 3(g). However, cytokinesis did not occur after several hours as shown in Figure 3(h).

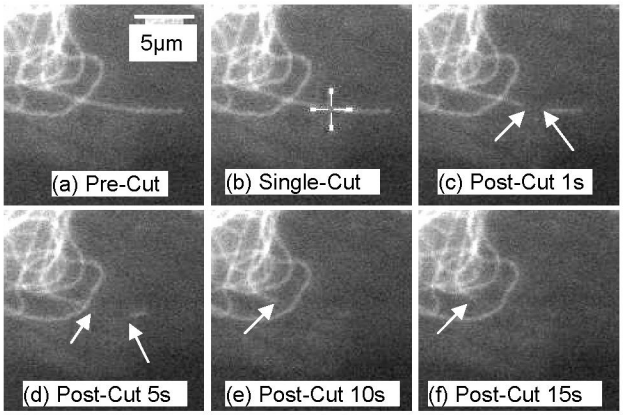

Figure 2 Femto-second laser exposure and effects on single microtubule. (a) Fluorescent image before laser exposure. (b) Crosshairs depict exact location of laser focal point during laser exposure. (c-f) Images captured immediately after laser exposure show a loss of fluorescence in the targeted region.

C. *Internet-based laser ablation control*

The robotic laser ablation microscope system can be operated via the internet using most internet accessible devices, including laptops and desktop computers. Some examples have been given in (10). The experiment testing irregular shape cutting through the internet was conducted from New York City using the *Logmein.com* web server as shown in Figure 4. Red blood cells were deposited on a

microscope cover glass, allowed to air-dry, and mounted in a rose chamber (20). The user can draw multiple different shapes on the captured image. The user can also modify the ablation power and the ablation distance between the two ablation spots in the front panel of RoboLase (Figure 1). The irregular shapes were cut out with the ablation distance smaller than the actual ablation radius (3μm) at high laser power as shown in Figure 4 (a). The discrete ablation spots can be clearly seen with bigger ablation distance at high laser power (Figure 4 (b)) and at low laser power (Figure 4(c)). The patterns (MB and NYC) can also be laser-etched via the internet as shown in Figure 4(d).

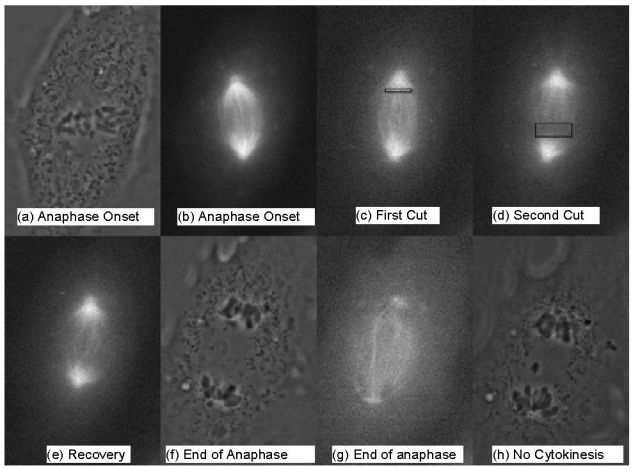

Figure 3 Anaphase spindle cutting using pico-second laser (532nm). (a) Anaphase onset shown in phase contrast image. (b) Fluorescence image of anaphase onset. (c) Fluorescent image after the first cut. (d) Fluorescent image after the second cut. (e) Fluorescent image during recovery. (f) Phase contrast image at end of anaphase. (g) Fluorescent image at end of anaphase. (h) No cytokinesis after several hours.

III. Robotic Laser Trapping Microscope System

A. System setup

The detailed hardware setup of the robotic automatic tracking and trapping system was described in (5). Analysis of sperm motility is the main application of this system. Briefly, thawed cryogenically frozen or fresh sperm of different species were suspended at 30,000 sperm per milliliter in buffered saline with bovine serum albumin media. Suspensions were injected into 2 mm deep rose chambers. The hardware system for the laser trapping mode is very similar to the laser cutting mode except the laser trapping source is a Nd:YVO4 continuous wave 1064 nm wavelength laser (Newport, BL-106C, Newport, CA) and the camera is a RS-170 standard CCD camera (Model XC-75, Sony, Japan) digitized by an image acquisition board (NI PXI-1407, National Instruments).

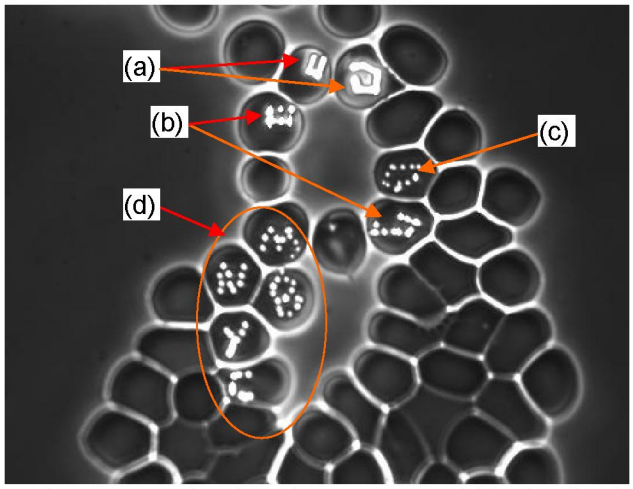

Figure 4 Irregular shape laser cuts on red blood cells via internet. (a) Irregular shapes using small ablation distance and high laser power. (b) Discrete ablation spots using bigger ablation distance and high laser power. (c) Closed shape ablated using bigger ablation distance and less laser power. (d) Patterns (MB and NYC) ablated (etched one letter per single red blood cell).

B. Species-dependant Sperm Image Processing

The measurement of sperm motility has been a major focus of basic and clinical sperm research for over 25 years. The robotic real-time automatic tracking and trapping system (RATTS) is used to quantify the motility and swimming force of sperm using video rate tracking and automated laser trapping. Single sperm trapping studies require a high NA oil immersion objective lens, which characteristically has a very shallow depth of field (a few microns). As a result, swimming sperm routinely move in and out of focus as contrasted to imaging with a low NA air immersion objective lens. Dog sperm were initially used to develop the tracking algorithm. The background was dynamically subtracted, multi-thresholding method and speed-check feature were applied, and collision detection was considered in the off-line single sperm tracking algorithm, SSTA (4). Sperm motility of other species can also be analyzed using SSTA or RATTS. However, different sperm shapes appear differently under the phase contrast illumination. For instance, the head of dog sperm is round and the mid-piece is short. In the phase contrast image of dog sperm, only a bright sperm head is presented (Figure 5). On the contrary, the head of mouse sperm is flat and the mid-piece is long and thick. Therefore, both the head and mid-piece are presented in the phase contrast illumination (Figure 6). The center of the thresholded mouse sperm image may not indicate the center of the sperm head, which may not only reduce the swimming speed calculation, but also make laser trapping impossible (the 3-D stable laser trap can only be generated when the sperm head is under the laser focus spot). In order to successfully track and trap sperm with large and bright mid-pieces, a head-prediction algorithm is used in SSTA and RATTS.

In Figure 6(a), at tracking frame N_i, using ParticalAnalysis function in Labview, the information, such as center coordinate (X_i, Y_i), orientation angle (θ_i, [0, 180°]), bounding rectangle width (W_i), height (H_i), and diagonal length (D_i) can be read out from the thresholded sperm image (Figure 6(b)). Note that (X_i, Y_i) can not represent the true center position of the sperm head since the bright mid-piece also appeared in the thresholded image. One of the two diagonal angles (θ or θ' in Figure 6(b)) is randomly chosen to be the orientation angle in Labview, so it can not be used alone to determine the swimming angle (ranging from 0 to 360°). In RATTS, the head prediction algorithm (user-selected for species with large and bright mid-pieces) will first determine the swimming direction of the sperm using the smoothed trajectory of the first N_{min} frames (N_{min} = 10 frames, the same as the setting in SSTA). The swimming angle α_{min} equals the orientation θ_{min} if the sperm is detected to be swimming upwards (swimming distance in Y direction: $\Delta Y_{min} = Y_{min} - Y_0 < -Y_{TH}$), and θ_{min} + 180° if the sperm is swimming down ($\Delta Y_{min} > Y_{TH}$). Note that the origin of the image is at the upper left corner. Y_{TH} is the threshold (set to 8μm in RATTS) to define that the sperm is swimming horizontally. For the horizontal swimming case ($-Y_{TH} < \Delta Y_{min} < Y_{TH}$), the swimming angle α_{min} should be in the range of [-90°, 90°] if it moves to the right (swimming distance in X axis, $\Delta X_{min} = X_{min} - X_0 > 0$) and [90°, -90°] if it moves to the left ($\Delta X_{min} < 0$).

After determining the swimming angle of the sperm at N_{min} frame, it is used to ensure the swimming angle α_i is θ_i or θ_i' in the following frame by defining the possible range [α_{i-1} - 70° , α_{i-1} + 70°]. Using the correct swimming angle α_i, the sperm head is predicted using the following equations

$$X_{i\text{-}HP} = X_i + \gamma D_i \cos(\alpha_i)$$

$$Y_{i\text{-}HP} = Y_i + \gamma D_i \sin(\alpha_i)$$

where γ is the user-defined prediction factor ranging from 0 to 1 (0.25 is chosen for mouse sperm in RATTS), and D_i is the diagonal length of the bounding rectangle (Figure 6(b)).

Note that it is very important to determine the swimming angle α_{min} in order to predict the sperm head correctly in the following frames. The swimming angle is postponed if the sperm does not move much in N_{min} frames (both $|\Delta Y_{min}| < Y_{TH}/2$ and $|\Delta X_{min}| < X_{TH}/2$, where $X_{TH} = Y_{TH}$).

The entire swimming trajectory (total of 402 frames) of the sperm in Figure 6 is shown in Figure 7. The swimming speeds were 77 μm/s and 72 μm/s with and without the head prediction respectively. Even though the difference between the two swimming speeds is less than 10%, head prediction is critical for the laser trapping application. Without head prediction, (X_{402}, Y_{402}) is detected as the sperm center which will most likely cause the sperm to be scattered by the laser when the laser shutter is opened. However, when head prediction, ($X_{402\text{-}HP}$, $Y_{402\text{-}HP}$) is detected as the sperm center, this will lead to a higher percent chance of successfully sperm trapping.

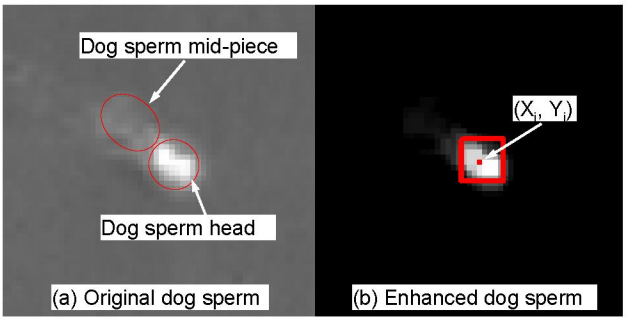

Figure 5 Dog sperm image before and after head prediction. (a) Original phase contrast image with bright head and dark mid-piece. (b) Enhanced image with rectangle to bound the thresholded sperm image, (X_i, Y_i) represents the center of the sperm head

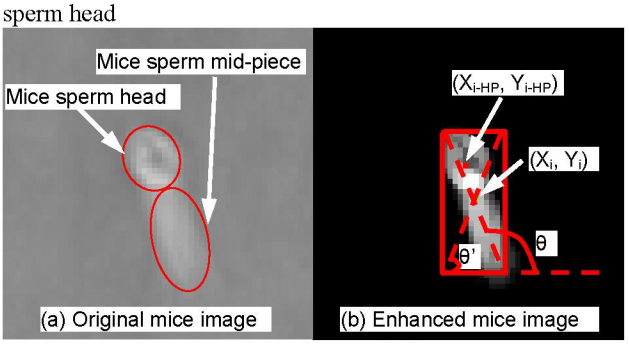

Figure 6 Mouse sperm image before and after head prediction. (a) Original phase contrast image with bright head and mid-piece. (b) Enhanced image with rectangle that bounds the thresholded sperm. (X_i, Y_i) represents the center of the sperm without head prediction, ($X_{i\text{-}HP}$, $Y_{i\text{-}HP}$) represents the center of the sperm with head prediction. The orientation angle θ_i and θ_i' are the two possible readouts from Labview

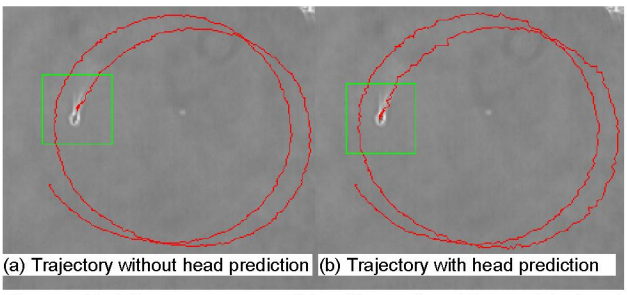

Figure 7 Mouse sperm with (b) and without (a) head prediction. The square represents the ROI at Frame 402

C. *Internet-based laser trapping control*

The robotic automatic tracking and trapping system can also be accessed through the internet (Logmein.com server) as showed in Figure 8. Collaborators from the University of Queensland, Brisbane, Australia accessed RATTS. Dog sperm were loaded into a rose chamber and onto the microscope in San Diego. Images of the sperm swimming were seen in Australia through the internet. One of the collaborators in Australia clicked on a swimming sperm "of-choice" (Figure 8(a)) to initialize the real-time automatic sperm tracking for

the next 5 seconds. The sperm was then relocated to the laser trap position and held under the trap for 10 seconds (Figure 8(b)).

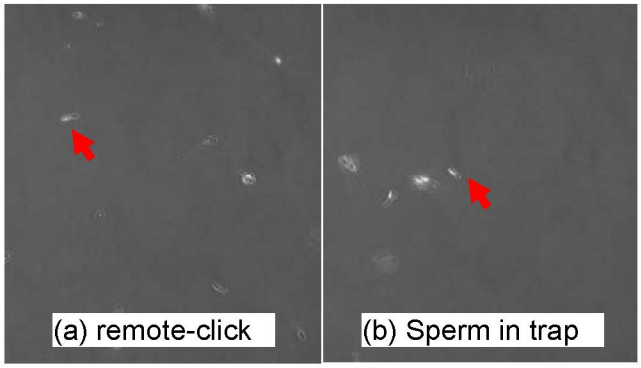

Figure 8 Remote-control of real-time sperm tracking and trapping system. (a) Guest from Australia clicked on a selected swimming dog sperm on the image screen in Australia which then activated RATTS in the UCSD lab. (b) The same sperm in (a) was held in the laser trap after tracking it for 5 seconds. It was trapped for 10 seconds.

IV. Conclusions

In this paper, the structure and features of the robotic laser scissors and laser tweezers microscope system are presented. The robotic laser ablation microscope system can be used to cleanly ablate a single microtubule or both half spindles after anaphase onset of live cells, and the microtubule depolymerization rate and the prevention or delay of cytokinesis can be observed respectively. The robotic automatic tracking and trapping system can be used to study sperm motility. Based on the species-dependent sperm "track & trap" problem, a head prediction algorithm is described for the species with large and bright mid-pieces in order to increase the success of laser trapping. It is also shown that both laser scissors and laser tweezers systems can be accessed through the internet using the Logmein server, which makes it feasible to perform biological experiments with the collaborators throughout the world.

References

[1] A. R. Cohen, B. Roysam, J. N. Turner, "Automated tracing and volume measurements of neurons from 3-D confocal fluorescence microscopy data," J Microsc. 1994 Feb;173(Pt 2):103-14

[2] W. He, T. A. Hamilton, A. R. Cohen, T. J. Holmes , C. Pace, D. H. Szarowski, J. N. Turner and B. Roysam, "Automated Three-Dimensional Tracing of Neurons in Confocal and Brightfield Images," Microsc Microanal. 2003 Aug;9(4):296-310

[3] Z. Bao, J. I. Murray, T. Boyle, S. L. Ooi, M. J. Sandel, and R. H. Waterston, "Automated cell lineage tracing in Caenorhabditis elegans," Proc Natl Acad Sci U S A. 2006 February 21; 103(8): 2707–2712.

[4] L. Z. Shi, J. M. Nascimento, M. W. Berns, E. L. Botvinick, "Computer-based tracking of single sperm," J. Biomed Opt, Sept-Oct, 2006

[5] L. Z. Shi, J. M. Nascimento, C. Chandsawangbhuwana, M. W. Berns, E. L. Botvinick, "Real-time Automated Tracking and Trapping System (RATTS) for Sperm," Microsc Res Tech. 2006 (69(11): 894-902.

[6] S. Yeom, B. Javidi, "Automatic identification of biological microorganisms using three-dimensional complex morphology," J Biomed Opt. 2006 Mar-Apr;11(2):024017

[7] J. Bloem, M. Veninga, J. Shepherd, "Fully Automatic Determination of Soil Bacterium Numbers, Cell Volumes, and Frequencies of Dividing Cells by Confocal Laser Scanning Microscopy and Image Analysis," Appl Environ Microbiol. 1995 Mar;61(3):926-936

[8] G. W. Brodland, J. H. Veldhuis, "Three-dimensional reconstruction of live embryos using robotic macroscope images," IEEE Trans Biomed Eng. 1998 Sep;45(9):1173-81

[9] W. Lin, J. Wilder, S. Grossman, D. J. Foran, "A network-reactive model for distributed telemicroscopy," J Telemed Telecare. 2003;9(2):78-83

[10] E. L. Botvinick, M. W. Berns, "Internet-based robotic laser scissors and tweezers microscopy," Microsc Res Tech. 2005 Oct;68(2):65-74

[11] J. Szymas, G. Wolf, W. Papierz, B. Jarosz, R. S. Weinstein, "Online Internet-based robotic telepathology in the diagnosis of neuro-oncology cases: a teleneuropathology feasibility study," Hum Pathol. 2001 Dec;32(12):1304-8

[12] V. Della Mea, P. Cataldi, B. Pertoldi, C. A. Beltrami, "Combining dynamic and static robotic telepathology: a report on 184 consecutive cases of frozen sections, histology and cytology," Anal Cell Pathol. 2000;20(1):33-9 Kaplan KJ,

[13] J. R. Burgess, G. D. Sandberg, C. P. Myers, T. R. Bigott, R. B. Greenspan, "Use of robotic telepathology for frozen-section diagnosis: a retrospective trial of a telepathology system for intraoperative consultation," Mod Pathol. 2002 Nov;15(11):1197-204

[14] C. G. Knight, A. Lorincz, A. Cao, K. Gidell, M. D. Klein, S. E. Langenburg., Computer-assisted, robot-enhanced open microsurgery in an animal model," J Laparoendosc Adv Surg Tech A. 2005 Apr;15(2):182-5

[15] W. Kuang, P. R. Shin, M. Oder, A. J. Thomas Jr., "Robotic-assisted vasovasostomy: a two-layer technique in an animal model," Urology. 2005 Apr;65(4):811-4

[16] P. N. Prasad, Introduction to biophotonics, John Wiley & Sons, Inc., Hoboken, new Jersey, 2003.

[17] J. Conia, B. S. Edwards, S. Voelkel, "The micro-robotic laboratory: optical trapping and scissing for the biologist," J Clin Lab Anal. 1997;11(1):28-38

[18] N. M. Wakida, C. S. Lee, E. L. Botvinick, L. Z. Shi, A. Dvornikov, M. W. Berns, "Laser Nanosurgery of Single Microtubules Reveals Time and Location Dependent Depolymerization Rates," submitted to JBO, 2006.

[19] N. M. Baker, E.L. Botvinick, Linda Z. Shi, George Wu, M.B. Berns, "Mitotic spindle studied using laser scissors," SPIE, SPIE Optics & Photonics conference in August 2006, San Diego, 6326.

[20] M. W. Berns E. L. Botvinick, L. Liaw, C-H Sun, J. Shah, "Micromanipulation of chromosomes and the mitotic spindle using laser microsurgery (laser scissors) and laser-induced optical forces (laser tweezers)," In: Celis J, editor. Cell biology: a laboratory handbook. Burlington, MA: Elsevier Press, 2005.

[21] J. M. Nascimento, E. L. Botvinick, L. Z. Shi, B. Durrant, and M. W. Berns, "Analysis of sperm motility using optical tweezers," J Biomed Opt, July-August, 2006.